ISSN 2354-9114 (online), ISSN 0024-9521 (print)
Indonesian Journal of Geography Vol 55, No 2 (2023): 235-247
DOI: 10.22146/ijg.81306 website: https://jurnal.ugm.ac.id/ijg

INDONESIAN JOURNAL OF GEOGRAPHY

REVIEW ARTICLE

Spatio-Temporal Variations of Reference Evapotranspiration in Western Iran

Yaser Sabzevari[1], Saeid Eslamian[2*]
[1,2]Water Department, Agricultural College, Isfahan University of Technology

Received: 2023-01-13
Revised: 2023-03-10
Accepted: 2023-05-10

Keywords:
Evapotranspiration, Reference Plant, Spatial Distribution, temporal changes, GIS.

Corresponding email:
saeid@iut.ac.ir

Abstract. Optimal management of water resources requires accurate determination of water balance components in each region and Evapotranspiration is one of the most important components of water balance. The purpose of this study was to investigate the spatiotemporal variability of reference evapotranspiration in Lorestan province- western Iran country using the Man-Kendall test and GIS then assess the effect of different climatic parameters on ET0 using multivariate regression. Lorestan province with a 28064 km area in western Iran has 9 synoptic stations including Khorramabad, Boroujerd, Aligouderz, Azna, Doroud, Koohdasht, Poldokhter, Aleshatar, and Noorabad. In this study, meteorological data were used for 9 synoptic stations of the Lorestan in a period from 2001 to 2017. The results showed that at most of the stations and most months, the changing trend was decreasing. The annual decrease in Azna station with Z=-2.73 at 99% level, and in the stations of Aligodarz, Kohdasht, and Doroud with Z equal to -2.27, -2.35, and -2.2, respectively at 95% was significant. The spatial distribution of ET0 showed that the maximum amount of ET0 occurred in the south of Lorestan Province, and decreased from south to north and west to east of the study area. These results indicate the influence of latitude and altitude on the spatial distribution of ET0. The impact of different parameters showed the greatest effect of maximum temperature and wind speed on ET0.

1. Introduction

Iran has an arid and semi-arid climate. In this country due to rainfall in seasons outside of cultivation and inappropriate spatial distribution, does not meet the requirements of water resources in different sectors (Mehdizadeh et al., 2017). Therefore, to deal with the water crisis in this condition, the management of available resources is essential. Optimal management of water resources requires accurate determination of water balance components in each region for each year. Evapotranspiration, which includes evaporation from the surface of water or wet soil, and transpiration from the surface of vegetation, is one of the most important and effective components of water balance in any region. Due to the variability of evapotranspiration for different plants in different conditions, first, the reference evapotranspiration (ET0) is calculated, and then from it and using plant coefficients the rate of evapotranspiration of the plant can be estimated (de Oliveira et al., 2021). According to the FAO standard, ET0 is the amount of water that a plant covered with a particular plant (such as grass or alfalfa) consumes over some time so that the field is not deficient in water during the growing season (Paredes et al., 2020). Therefore, to estimate evapotranspiration from the surface of any vegetation, ET0 must be calculated reliably. There are different methods for calculating ET0, each of which often gives different results depending on the different meteorological conditions (Grismer et al., 2002). Numerous studies around the world show the accuracy of the results of the FAO-penman-monteith model in different climatic conditions (Djaman et al., 2015). Spatial distribution and temporal variation of ET0 are one of the most important components of water balance (Nam et al., 2015). Tabari et al. (2011) examined the ET0 trend in 20 synoptic stations in the west of Iran. The results showed that in 70% of the stations, the ET0 trend was increasing on an annual scale and also more increasing trends occurred in winter and summer. Zongxing et al. (2015) investigated the temporal and spatial variations of ET0 in southwest China. The results showed the effect of temperature and wind speed parameters in the distribution and increase of ET0. de Oliveira et al. (2021) investigated the temporal changes of reference evapotranspiration with emphasis on land use change in the southern Amazon basin. The results showed that reference evapotranspiration has a significant trend in only one station located in Kanarana city with a negative trend of 8.4 mm/year, and the variable that had the greatest effect on ETo was solar radiation. Zhao et al. (2022) Simulated changes in evapotranspiration on a regional scale. The results showed that the spatial distribution of ET is influenced by both natural factors (eg, land cover types) and human activities (eg, groundwater extraction, and planted crops). Prăvălie et al. (2019) examined the temporal changes of the climate balance in response to the precipitation and ET0 trend in the period 1961-2013 in Romania. The results showed a decrease in the climate balance due to a decrease in precipitation and an increase in ET0 during the study period. Nsiah et al. (2021) assessed the spatial changes of evapotranspiration in the Pra River Basin of Ghana. The spatial variation of ET was higher in the western, central, and eastern parts of the basin, but it was lower in the northern part and parts of the southern part of the basin where there are many settlements and forests. Areas with

high temperature and high solar radiation experience high ET, while low wind speed, low to moderate temperature, and low to moderate solar radiation experience low ET. Linear regression analysis showed a good fit with an R^2= 0.93, indicating that 93% of the variation in observed field-measured ET perfectly matched the ET distributions produced by the SEBAL model. Samuel et al. (2018) examined the spatiotemporal changes of ET0 in Ethiopia. The results showed that the amount of ET0 during the study period depended on temperature, surface radiation, soil moisture content, and crop growth stage. Wang et al. (2018) examined the temporal and spatial changes of ET0 in Hebei Province, China. The results showed a great spatial heterogeneity of ET0 in the area covered by forests. Lu et al. (2020) studied the variations in evapotranspiration during various seasons in the Chinese Genhe River Basin. The total evapotranspiration during the growing seasons was significantly higher than it was during the freezing-thawing periods. Temperature and precipitation were the main determinants of evapotranspiration. Tang and Tang (2021) examined from1975 to 2014 the Variations and Influencing Factors of Potential Evapotranspiration in Large Siberian River Basins. The PET trends are typically not significant. The significance of wind speed in PET estimates in the Siberian River basins is highlighted by this finding. Chang et al. (2023) studied the Variations in Evapotranspiration of the Tibetan Plateau between 1982 and 2015. The spatiotemporal changes of ET showed that from the southeast to the northwest of the Tibetan Plateau, the multiyear mean annual ET decreased, while the averaged ET and its components increased noticeably at seasonal and annual scales. Shao et al. (2022) investigated the seasonal variation and influencing factors of evapotranspiration over a "floating blanket" wetland in southwest China. Results indicated that monthly net radiation had the greatest influence on ET, and that there was a significant inverse relationship between annual ET and precipitation. Wang et al. (2022) investigated the spatiotemporal changes in evapotranspiration and its effect factors in the semiarid Hailar river basin, in Northern China. The results indicated that a definite upward trend and significant spatial heterogeneity can be seen in the annual spatial distribution of ET. Sensitivity and influential factor contribution analyses reveal that climate warming, followed by precipitation, is the primary driver of interannual variability in ET. Fu et al. (2022) studied the spatiotemporal changes of terrestrial evapotranspiration in China from 2000 to 2019. for the study, the average annual ET grew at a 5.3746 mm yr^{-1} ($P < 0.01$) rate. The trend is primarily driven by rising precipitation and wind speed. Liu et al. (2022) In a karst basin in southwest China, investigated spatiotemporal variations in evapotranspiration in response to alterations in the local environment and vegetation. In regions with low altitudes and lots of precipitation, temperature and wind speed showed positive correlations with ET.

Based on the researches, it seems estimating the reference evapotranspiration is a necessity for planning water requirements in agriculture, designing irrigation systems and optimal management of water resources. Due to the effect of climate change, and spatial conditions on the distribution of reference evapotranspiration, it is necessary to study the changes of this parameter over time and place for each region. in these studies, statistical or mathematical methods are often used to investigate temporal-spatial changes. The combined use of methods that examine temporal and spatial changes that can evaluate the impact of geographic conditions simultaneously with temporal changes and the impact of different climatic parameters on evapotranspiration is considered as a gap in these studies for a better comparison. Therefore, the purpose of this study was to investigate the temporal and spatial changes of reference evapotranspiration using Geographic Information System (GIS) and Mankendall test and to investigate the effect of meteorological parameters on it, using multivariate regression In Lorestan province in western Iran. for this purpose, First, changes in the time trend of ET_0 changes are checked with the Mankendall test, and then with the help of GIS, the influence of geographical conditions on the temporal and spatial changes of ET_0 in different months in the study area is examined. Finally, using multivariate regression, the effects of different climatic parameters on these changes are evaluated.

2. Material and Methods

Study area

Lorestan province with a 28064 km area in western Iran is located between 46° 51′ to 50° 3′ east longitude of the Greenwich meridian and 32° 37′ and 34° 22′ north latitude of the equator. Its height from sea level varies from the highest point in the north of Lorestan with an altitude of 4050 m to the lowest point in the south with an altitude of 500 meters. The average long-term rainfall in Lorestan is 498.6 mm and the highest monthly rainfall is in April with 86.4 mm. 43% of the province's rainfall occurs in winter, 29.5% in autumn, and 27% in spring. The average long-term maximum and minimum temperatures in Lorestan are 22.6 and 7.7 ° C, respectively. The highest and lowest long-term mean temperatures are related to Poldokhtar station in the south and Noorabad station in the north of Lorestan with values of 22.8 and 11.9 ° C, respectively. The hottest and coldest months of the province are August and January, respectively. According to available statistics, the long-term average relative humidity of Lorestan is 66.2%, while Poldokhtar with 37.2% has the lowest average relative humidity, respectively. Among the months of the year, February with 66.2% is the wettest month, and August with 25.1% is the driest month of the year. The long-term average number of sunshine hours in Lorestan is 3029.6 hours and Koohdasht in the southwest of Lorestan with an average of 3205.2 hours and Aligoudarz in the east of Lorestan with an average of 2749.7 hours has the highest and lowest number of sunshine hours in the Lorestan, respectively. July with an average of 351.3 hours had the most and January with an average of 167.4 hours had the least sunshine hours. Table 1 shows the latitude and longitude, height, long-term average meteorological statistics, and climatic classification based on the Amberjeh climate in 9 synoptic stations of Lorestan province. Figure 1 shows the geographical location of Lorestan province and its synoptic stations in Iran country.

In this study, to calculate the reference evapotranspiration using the FAO-Penman-Monteith method and to investigate its trend by the Man-kendall test and its interpolation with GIS and to investigate the effect of meteorological parameters on it, the maximum temperature, Minimum temperature, maximum relative humidity, minimum relative humidity, sunshine hours and wind speed (at height of two meters), in a period from 2001 to 2017 in monthly scale were used.

Table 1. Geographical and climatic characteristics of synoptic stations in Lorestan province

station	Amberjeh	Sun. hour	Avg. hum.	Avg. temp.	Pre.	Height (m)	longitude	latitude
Aleshtar	Cold semi-dry	3072.8	53	13	444.7	1567	´15 °48	´49 °33
Boroujerd	Cold semi-dry	3033.4	42	14.7	456.4	1629	´45 °48	´35 °33
Aligoudarz	Cold dry	2749.7	40	12.4	387.3	2022	´42 °49	´24 °33
Doroud	Cold dry	3091	40	16.2	631.7	1527	´94 °49	´29 °33
Noorabad	Dry heat	2950.9	47.5	11.9	467.9	1860	´99 °48	´03 °34
Azna	Cold semi-dry	3088.2	50.5	12.4	411.6	1872	´25 °49	´27 °33
Khorramabad	Wet cold	2959.1	41	17.2	500.1	1148	´17 °45	´26 °33
Poldokhtar	Cold semi-dry	3116.1	37.2	22.8	360.1	713	´43 °47	´09 °33
Koohdasht	Cold semi-dry	3205.2	48.7	15.9	366.7	1198	´39 °47	´31 °33

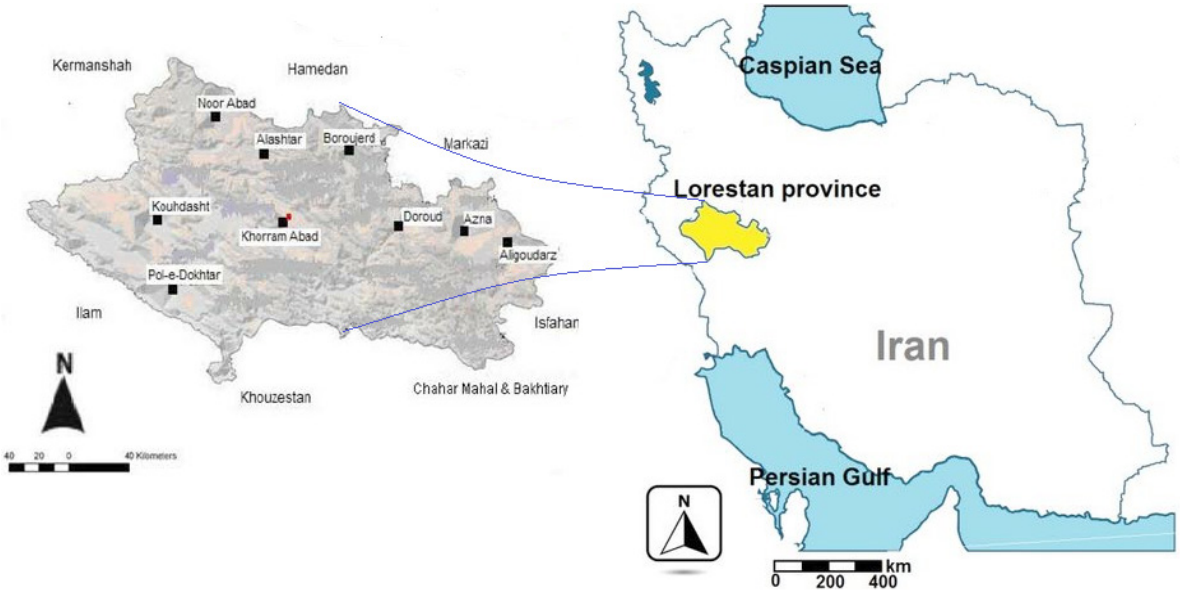

Figure 1: Geographical location of Lorestan province and its synoptic stations

Calculation of reference evapotranspiration by FAO-Penman-Monteith method

In 1990, the International Commission on Irrigation and Drainage (ICID) and the World Food Organization (FAO) introduced the FAO-Penman-Monteith method as the only standard method for calculating ET0 according to Climatic data (Hargreaves, 1994). This method requires data on radiation, temperature, humidity, and wind speed and has been able to provide an accurate estimate of ET0 with a high degree of reliability in a wide range of regions and climates (Allen et al., 1998). In this study, to calculate ET0, the FAO-Penman-Monteith method was used as the standard method using RefET 3.2 software. The relation used to calculate ET0 is as follows:

$$ET_0 = \frac{[0.408(R_n - G) + [(900\gamma)/(T+273)] \times U_2 \times (e_a - e_d)]}{\Delta + \gamma \times (1 + 0.34U_2)} \quad (1)$$

In this regard: ET0; reference Evapotranspiration, in terms of (mm / day) Rn; net radiation in terms of (MJ / m2 * day) G; Soil heat flux, in terms of (MJ / m2 * day) Δ; Slope of saturated steam pressure graph for temperature, in terms of (k_p / ^{0}c) γ; Psychometric constant, in terms of (k_p / ^{0}c) ea-ed; Lack of steam pressure at a height of 2 meters, in terms of (k_p), U2: Average daily wind speed at a height of 2 m above the ground, in terms of (m/s) T: The average daily air temperature at a height of 2 meters above the ground, in terms of (^{0}c).

ManKendall Test

The Mankendall test is used to check the time trend for each set of data. This test is based on non-parametric linear regression logic. The results of this test show whether there is a significant increase or decrease trend in a certain level of confidence in the time series trend. Using the Man-kendall nonparametric test is not sensitive to the normality of the data. The Man-Kendall test was first proposed by (Mann, 1945) and then developed by (Kendall, 1975). The use of this method was recommended by the World Meteorological Organization (Gibrilla et al., 2018). One of the strengths of the Man-kendall method is that it is suitable for time series that do not follow a specific distribution.

This method is used to examine the trend of data. In this method, the S statistic for the g_{th} month and the k_{th} station is calculated as follows:

$$Sgk = \sum_{i}^{n-1} \sum_{j=i+1}^{n-1} sgn\ (Xjgk - Xigk),\ \forall\ i<j\leq n \quad (2)$$

Where n is the number of series data and sgnθ is a function of the sign and θ is the difference between the two observations in each of the studied parameters in different years i and j, which are as follows Defined:

$$Sgn(\theta) = \begin{cases} 1 & if \quad \theta > 0 \\ 0 & if \quad \theta = 0 \\ -1 & if \quad \theta < 0 \end{cases} \tag{3}$$

Man and Kendall showed that when n≥ 10, the S statistic is distributed almost normally and has a mean of 0 and the following standard deviation:

$$(\sigma gg)k = \frac{[n(n-1)(2n+5)-\sum d(d-1)(2d+5)]}{18} \tag{4}$$

Where d is the same amount of data in the time series. In this method, Sgk is normalized as follows:

$$S'gk = Sgk - sgn(Sgk) \tag{5}$$

Then the standardized test statistic or Z, which has a standard normal distribution with a mean of 0 and a variance of 1, is obtained as follows:

$$Zgk = \frac{S'gk}{(\sigma_{gg})}1/2 \tag{6}$$

If the value of Z is greater than ± 1.96, the data has a trend and the null hypothesis is rejected, otherwise, it has no trend. Z is the standard normal distribution statistic and is used in a two-domain test depending on the confidence levels of the item The test can take different values and S: is a parameter of the Mankendall method which is calculated It was mentioned above. The value of Z statistic for 95% and 99% confidence levels the percentages are considered to be 1.96 and 2.58, respectively.

Zoning methods

Kriging is a method of estimation that is based on the logic of weighted moving averages and is known as the best nonlinear estimator (Gaus et al., 2003). In this method, Z has a normal distribution. Otherwise, the nonlinear kriging method should be used or the variable distribution should be normalized. In this study, the Boxcox method was used to normalize abnormal data. The general relationship of kriging is as follows Equation 7:

$$Z^*(x_i) = \sum_{i=1}^{n} \lambda_i Z(x_i) \tag{7}$$

Where Z* (Xi) is: Estimated value of the variable in position Xi, λi is: the weight of sample i, and Z(Xi) is: the value of variables I, and n is the number of observations. to select the appropriate model, ordinary kriging, simple kriging, and universal kriging methods were implemented with all variance models available in the GIS software.

Inverse Distance Weighting (IDW) Method: This method is based on the principle that points with shorter distances have a variable value close to each other with more distances. In this method, for each of the measuring points, a weight is considered based on the distance between that point to the position of the unknown point. These weights are then controlled by the weighting power, so that the larger powers reduce the effect of points farther from the estimated point and the smaller powers distribute the weights more evenly between adjacent points. it should be noted that this method, regardless of the position and arrangement of points, only considers their distance, that is, points that have the same distance from the estimated point have the same weight (Yang et al., 2020). In this method, the amount of weight factor is calculated using the following formula:

$$\lambda_i = \frac{D_i^{-a}}{\sum_{i=1}^{n} D_i^{-a}} \tag{8}$$

in the above relation; λi: weight of station I, Di: distance of station I to the unknown point, and α: weighting power used in this study to the third power.

Global Polynomial Interpolation (GPI): This method is a multivariate regression model based on all data and creates an understanding level, and fits a model on the sampling points that can be a polygonal surface with Power: one, two, or four. The best application of this method is at levels with gentle and gradual changes (Antal et al., 2021).

Local Polynomial Interpolation (LPI): This method considers a short range of changes in the input data and is sensitive to neighborhood intervals in the shared window. As the window moves, the surface values in the center of each window at each point are estimated by fitting a polygon. This method has higher flexibility than the Global Polynomial Interpolation⁋ method. These two methods do not require any assumptions for the data.

Radial basis function (RBF): The functional radial is a function: Φj (X) = Φ (X-Xj) which depends on the distance between x = Rd and the fixed point Xj εRd. In this function, Φ is a continuous and dependent function of any ΩεRd subset. R represents the Euclidean distance between each pair of points in the set Ω. This method has 5 kernel functions: Regularized Completely Spline, Spline with Tension, Multiquadratic, Inverse Multiquadratic, and Plate Spline Thin (Antal et al., 2021).

Accuracy assessment

To evaluate the accuracy of each method or to select the appropriate parameter in them, there is a need for evaluation. There are several methods in this field, the most important method is the cross-validation method. In this method, comparisons are made between measured points and estimated values using specific methods. In this way, a point is deleted and the other point is estimated using this point and applying the desired interpolation method. This point is then returned to its place and the next point is removed, and so on for all points, an estimate is made so that at the end of the two columns there are observation values and estimated values that can be able to compare them. To evaluate the accuracy and error between the observed and estimated values, the root mean square error index (RMSE) was used to determine the appropriate method, which is known as an important indicator to show the accuracy of spatial analysis in GIS and through Equation 9 and using data Observations and predictions include:

$$RMSE = \sqrt{\frac{\sum_{i=1}^{n}((x_i) - (\overline{x}))^2}{n}} \tag{9}$$

In this method, one observation point is removed in each step and that point is estimated using the other observation points. This is repeated for all observation points, and at the, end there will be an estimate for each observation point. Among the various methods, the method with the lowest RMSE index is selected as the appropriate method.

Linear-multivariate regression model

With this method, several different variables can be analyzed. Multivariate regression, expresses the relationship between several predictor variables and the desired response variable. Such models have hypotheses. The assumptions that distinguish multivariate regression from simple regression are:

1. The number of predictor variables (independent) in the regression should be less than the number of observations.
2. There is a complete linear correlation between the predictor variables and response.

If the two assumptions are violated, the regression equation cannot be estimated. the matrix regression model can be represented as the following equation:

$$Y = X\beta + e \quad (10)$$

The β is a matrix of regression coefficients that are indeterminate coefficients that are responsible for estimating the response parameter, e is the fitting error matrix and Y is the response matrix. By solving equation (10) in terms of β we will have:

$$\beta = (X'X)^{-1}(X'Y) \quad (11)$$

In the above relation, X′ is the transposition of the matrix X. To calculate inverse (X′ X) the independent variables must not have much correlation, because in this case the matrix (X′ X) can not be inverted and increases the error in the effect Data rounding and calculations.

3. Results and discussion

Investigate the time trend of ET0

Table 2 shows the results of the Mankendall test to investigate the trend of ET0 changes.

ET0 Trend in months of the year

According to this table, in April, the ET0 trend has a positive slope in all stations except Poldokhtar, but the changes are not significant. There was no significant trend in May, but except in Khorramabad and Azna, in other stations the slope of the trend was positive. The trend of ET0 changes in June is such that most stations have a decreasing trend and in Azna station with z =-2.99 is significant at 99% and in Koohdasht with z= -2.5 is significant at the 95% level. The trend of changes in July for Azna and Aligoudarz stations with z = -2.23 and z = -2.31 was decreased by 95%. In August, the trend for Aleshtar and Aligoudarz stations at 99% level was increasing and decreasing with z = 2.58 and z = -2.9, respectively, and for Doroud with z = -2.35, It has been negatived at the 95% level. The trend of changes in September in Koohdasht and Azna stations is decreasing by 95% with z = -2.5 and z = -2.31. In October, the ET0 trend of Poldokhtar and Azna stations increased and decreased with statistics of 2.1 and -2.1, respectively, which are significant at the 95% level. Lorestan province ET0 trend has been decreasing in November, December, January, and February. This decrease in Koohdasht at the statistical level of 99% and in Azna at the statistical level of 95% in November, in Khorramabad in December at the level of 95%, in Dorud, Poldokhtar, and Azna at the level of 95% and in Aligoudarz at the level of 99% In February, it was significant. The trend in December was not significant. In the trend of changes in March, except in Khorramabad and Koohdasht, other stations had an increasing trend, which was significant in Noorabad with z = 2.1 at the level of 95.

ET0 Annual Trend in Studied stations

The trend of annual ET0 changes in Azna, Aligoudarz, Koohdasht, Doroud, Boroujerd, and Khorramabad stations has been decreasing and in Aleshtar, Noorabad, and Poldokhtar stations has been increasing, which has decreased in Azna station with the statistic of z =-2.73 at 99% level and in Aligoudarz, Koohdasht, and Doroud stations with statistics of -2.27, -2.35 and -2.2, respectively, significant at 95% level. Tabari et al. (2011) showed that in the west of Iran, the annual trend of ET0 was increasing and also more increasing trends occurred in winter and summer.

In general, it can be said that the trend of ET0 changes in the studied area has been decreasing. According to the

Table 2. Z statistical values of synoptic stations in Lorestan province in different periods

period	Aligoodarz	Azna	Poldokhtar	Koohdasht	Noorabad	Doroud	Boroujerd	Aleshtar	Khorramabad
April	0.76	0.22	0.15-	0	1.36	1.25	0.91	1.21	0.68
May	1.02	1.3-	0.41	0.83	1.13	0.87	0.8	0.5	0.5-
June	1-	2.9-	0.3	2.5-	0.68	0.34-	1.06-	0.5-	0.94-
July	2.31-	2.23-	1.48	1.85-	0.11-	1.85-	0.91	0.22	0.45-
August	2.9-	1.74-	0.6	1.6-	0.45	2.35-	0.11-	2.58	0.19-
September	6.1-	2.31-	0.7-	2.5-	0.26	1.32-	0.7	1.48	1.1-
October	0.7-	2.1-	2.1	1.74-	0.98	1.48-	0.91-	0.91	0.57-
November	1.6-	2.43-	0.5-	2.7-	0.98-	2-	1.67-	0.38-	0.94-
December	1.3-	1.9-	1.67-	1.44-	1.25-	0.76-	1.14-	1.29-	1.2-
January	1-	1.66-	1.74-	1.51-	1.55-	0.0-	0.87-	0.9-	2.08-
February	2.61-	2.35-	2.2-	1.78-	1.1-	2.42-	1.67-	1.13-	0.5-
March	1.02	0.38	0.3	0.19-	2.1	1.21	1.67	1.17	0.3-
Annual	2.27-	2.73-	0.07	2.35-	0.3	2.2-	0.45-	0.72	1.36-

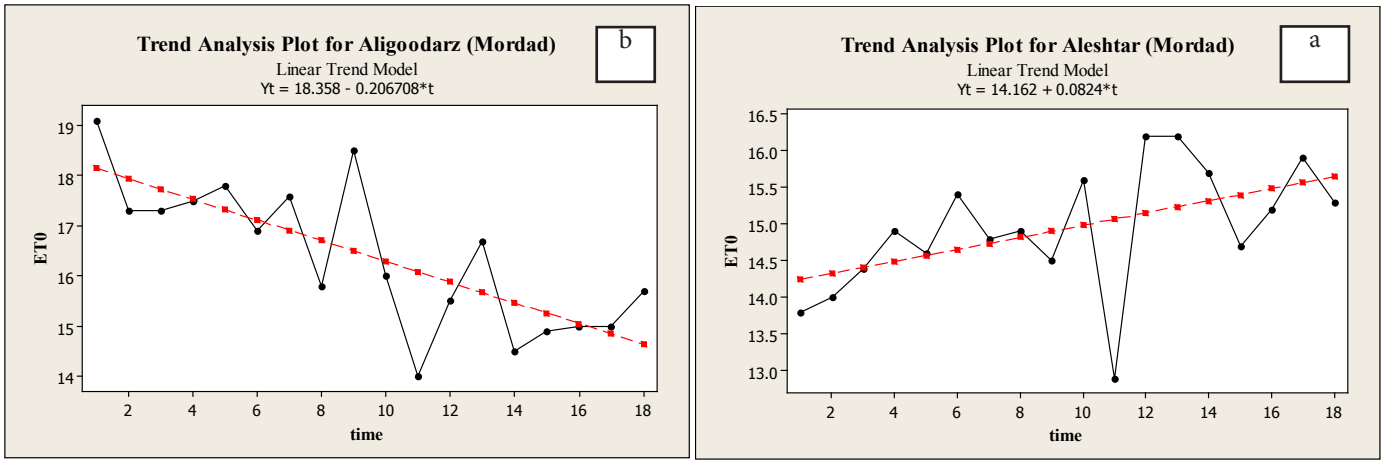

Figure 2: A- Chart of ET0 change trend in Aleshtar station in August, Figure 2- B- Chart of ET0 change trend in Aligoodarz station in August

statistics of all stations in different months, February has the lowest trend and April has the highest trend in ET0 changes. Among the 9 studied stations, Aleshtar station had the highest increase and Azna station had the lowest decrease in ET0 changes. de Oliveira et al. (2021) showed in the Amazon basin that reference evapotranspiration has a significant trend with a negative trend of 8.4 mm/year. Tang and Tang (2021) in Large Siberian River Basins showed that The PET trends are not significant between 1975 and 2014.

Figure 2-a shows the trend of ET0 changes in Aleshtar station in August as the most increasing trend and Figure 2-b shows the trend of ET0 changes in Aligoudarz station in August as decreasing trend. As can be seen from these graphs, the trend slope in August for Aleshtar station is increasing with a slope of 0.08%, and for Aligoudarz station with a slope of -0.2% is decreasing.

Investigation of the spatial distribution of ET0

Different interpolation methods were used to study the spatial variations of ET0 in Lorestan province in the west of Iran. Also, to study its temporal changes, monthly and annual changes in 2000 and 2017 were examined.

Select Best Interpolation Methos

Cross-validation was used to select the appropriate interpolation method. The results of examining the accuracy of various kriging methods with different semi-variables, IDW with powers 1, 2, and 3, GPI, LPI, and RBF are given in Table 3. Based on this table, the Simple Kriging (J-Bessel) method for ET0 interpolation in May, June, July, August, October, December, January, March, and annually with RMSE values of respectively. 1.34, 1.93, 2.01, 2.04, 0.74, 0.38, 0.48, 0.54, and 0.93, in 2000, and June, July, September, October, and annually with RMSE values of 1.34, 1.96, 1.96, 0.91, and 0.97, respectively, were selected in 2017. LPI method for interpolation in April, November, December, January, February, and March with RMSE values of 0.62, 1.06, 0.28, 0.54, 0.45, and 0.76, respectively in 2017, Simple Kriging (Hole Effect) method for interpolation in April, September, and February with RMSE values of 0.36, 1.18 and 0.34, respectively, in 2000, Simple Kriging (Rational Quadratic) method for interpolation in November 2000 with RMSE equal to 0.83 and August 2017 with RMSE equal to 2.27 and RBF method for interpolation in May 2017 with RMSE 0.84 was selected as the most suitable models. According to these results, in general, it can be said that the Simple Kriging method has been more accurate than other methods.

ET0 Zonation

After selecting the appropriate interpolation method, ET0 was zoned in Lorestan province. Figure 3 shows the ET0 zoning maps in the twelve months of the year and its annual value in both 2000 and 2017. Accordingly, the maps show a specific trend in the spatial distribution of ET0 in the study area. According to the maps, the maximum amount of ET0 occurs in the south of Lorestan and has decreased by moving to the north and east of the province. Poldokhtar city is located in the south of the province, and has the lowest height in the province. Also, the eastern and northern regions of the province, which are located in Aligoudar and Noorabad, are considered the highest areas of Lorestan. On the other hand, moving to the north of Lorestan, the latitude increases. From these interpretations, the effect of spatial conditions through latitude and height on ET0 changes is realized and it is observed that with increasing latitude in the area, the rate of ET0 has decreased. The spatial distribution trend in April, May, June, October, November, December, February, and March 2000 has been such that the highest amount of ET0 in the south and in January in the northeast, and the lowest amount in the north and it happened in the east of the province. In 2017, in these months, the increasing range has been extended to the east and the decreasing range has been extended to the west of the study area. The spatial distribution of ET0 in August 2000 was the same as the mentioned months, in which in 2017, except for parts of the north and northeast, the rest of the province had the maximum ET0. In July and September of 2000, the highest amount of ET0 occurred in the south, center, and north of the area, and 2017 in the center and south of the area. The annual spatial distribution of ET0 in 2000 was like most months of the year, so the highest value was in the south and the lowest value in the east and north of the province. In 2017, the same pattern occurred in the distribution of ET0 by this difference that data is reduced. Nsiah et al. (2021) showed a variation of ET was higher in the western, central, and eastern parts of the Pra River Basin of Ghana, but it was lower in the northern and southern parts of the basin where there are many settlements and forests. Chang et al. (2023) showed that in Tibetan Plateau's from the southeast to the northwest the multiyear mean annual ET decreased.

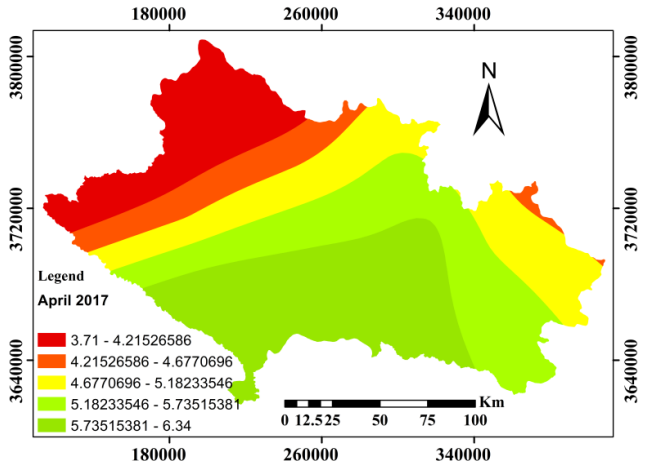
180000
260000
340000
3800000
3720000
3640000
N
Legend
April 2017
3.71 - 4.21526586
4.21526586 - 4.6770696
4.6770696 - 5.18233546
5.18233546 - 5.73515381
5.73515381 - 6.34
0 12.525 50 75 100
Km

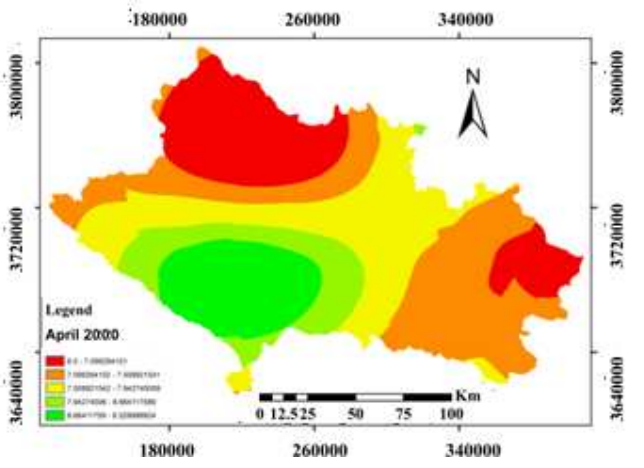
180000
260000
340000
3800000
3720000
3640000
N
Legend
April 2000
0 12.525 50 75 100
Km

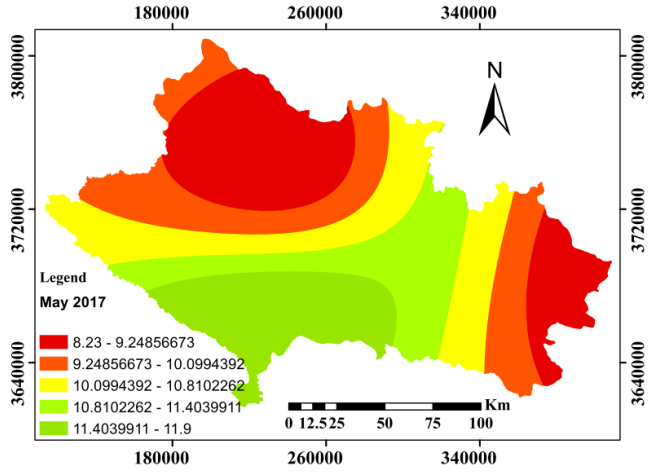
180000
260000
340000
3800000
3720000
3640000
N
Legend
May 2017
8.23 - 9.24856673
9.24856673 - 10.0994392
10.0994392 - 10.8102262
10.8102262 - 11.4039911
11.4039911 - 11.9
0 12.525 50 75 100
Km

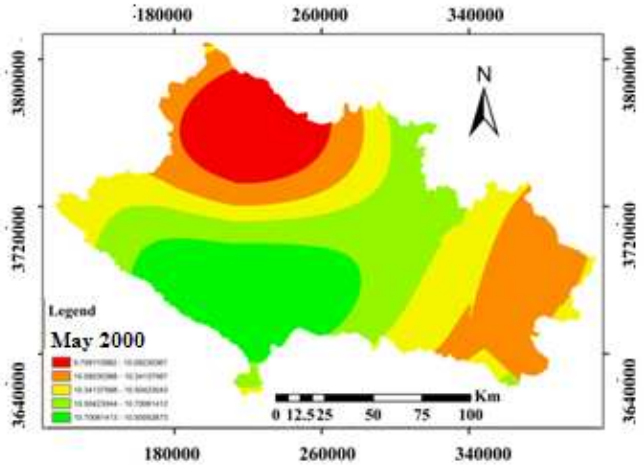
180000
260000
340000
3800000
3720000
3640000
N
Legend
May 2000
0 12.525 50 75 100
Km

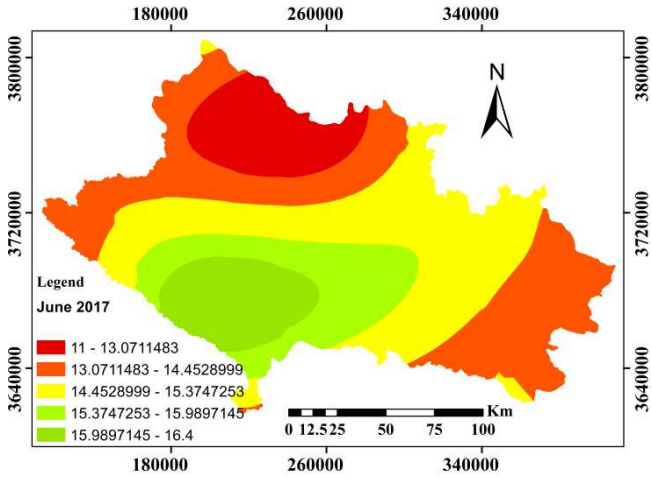
180000
260000
340000
3800000
3720000
3640000
N
Legend
June 2017
11 - 13.0711483
13.0711483 - 14.4528999
14.4528999 - 15.3747253
15.3747253 - 15.9897145
15.9897145 - 16.4
0 12.525 50 75 100
Km

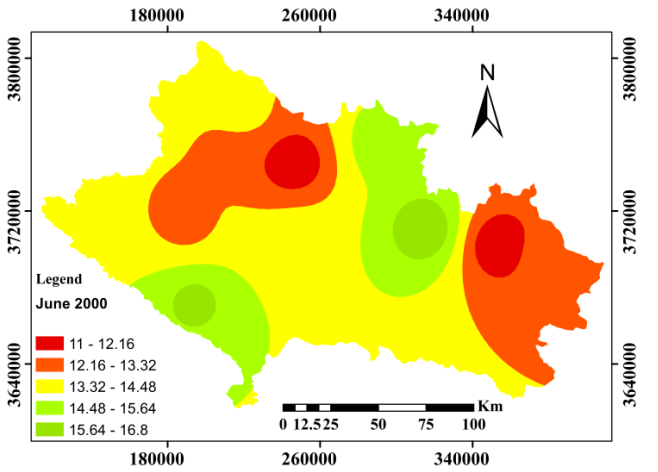
180000
260000
340000
3800000
3720000
3640000
N
Legend
June 2000
11 - 12.16
12.16 - 13.32
13.32 - 14.48
14.48 - 15.64
15.64 - 16.8
0 12.525 50 75 100
Km

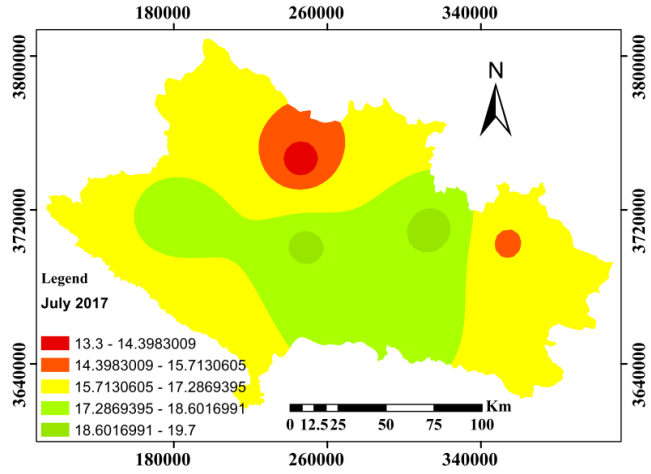
180000
260000
340000
3800000
3720000
3640000
N
Legend
July 2017
13.3 - 14.3983009
14.3983009 - 15.7130605
15.7130605 - 17.2869395
17.2869395 - 18.6016991
18.6016991 - 19.7
0 12.525 50 75 100
Km

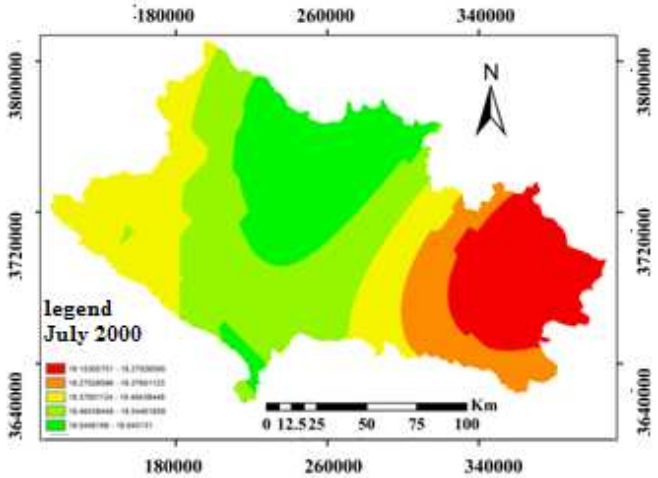
180000
260000
340000
3800000
3720000
3640000
N
legend
July 2000
0 12.525 50 75 100
Km

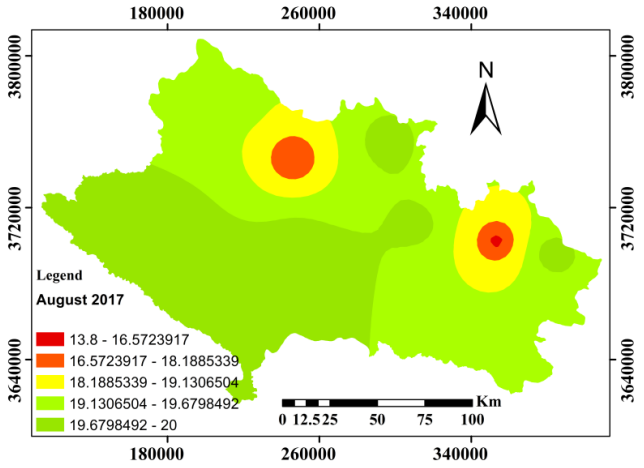
180000
260000
340000
3800000
3720000
3640000
N
Legend
August 2017
13.8 - 16.5723917
16.5723917 - 18.1885339
18.1885339 - 19.1306504
19.1306504 - 19.6798492
19.6798492 - 20
0 12.525 50 75 100
Km

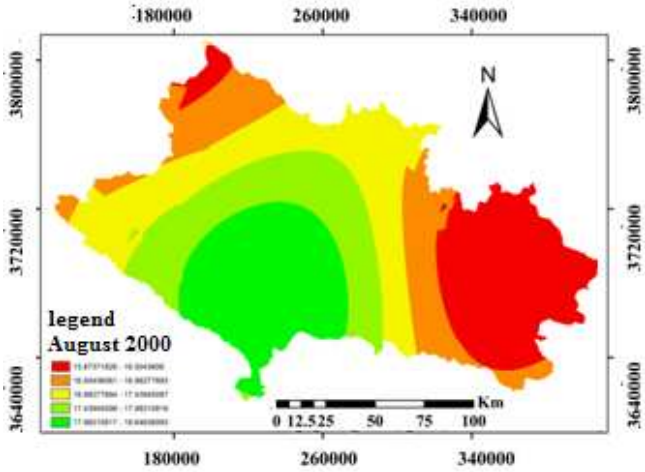
180000
260000
340000
3800000
3720000
3640000
N
legend
August 2000
0 12.525 50 75 100
Km

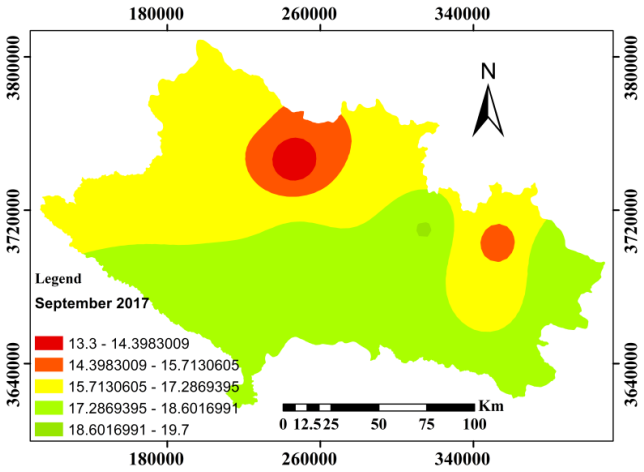
180000
260000
340000
3800000
3720000
3640000
N
Legend
September 2017
13.3 - 14.3983009
14.3983009 - 15.7130605
15.7130605 - 17.2869395
17.2869395 - 18.6016991
18.6016991 - 19.7
0 12.525 50 75 100
Km

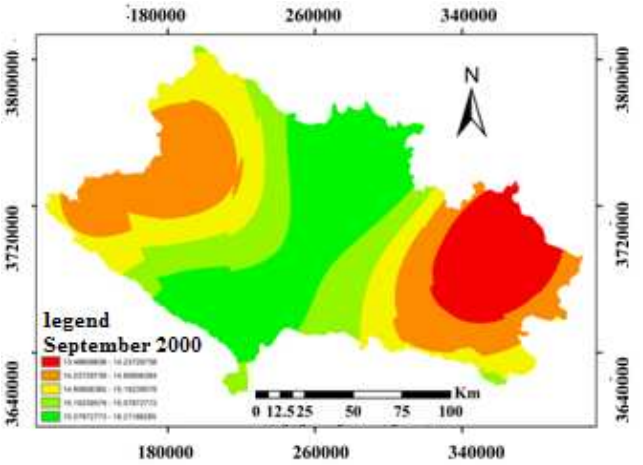
180000
260000
340000
3800000
3720000
3640000
N
legend
September 2000
0 12.525 50 75 100
Km

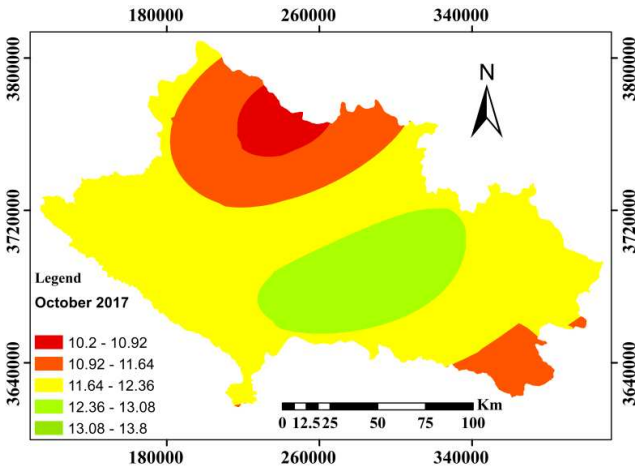
180000
260000
340000
3800000
3720000
3640000
N
Legend
October 2017
10.2 - 10.92
10.92 - 11.64
11.64 - 12.36
12.36 - 13.08
13.08 - 13.8
0 12.525 50 75 100
Km

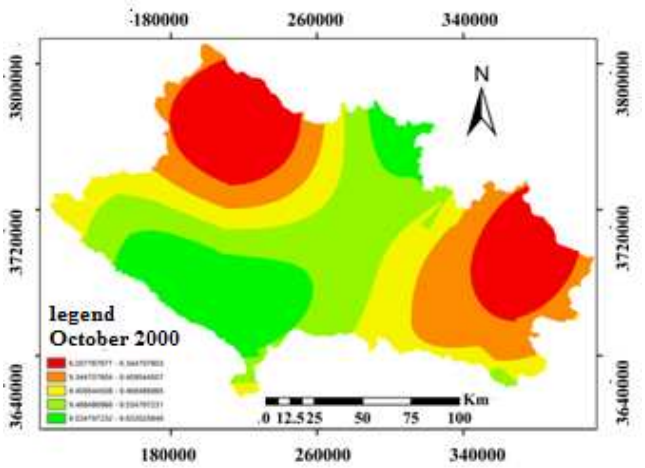
180000
260000
340000
3800000
3720000
3640000
N
legend
October 2000
0 12.525 50 75 100
Km

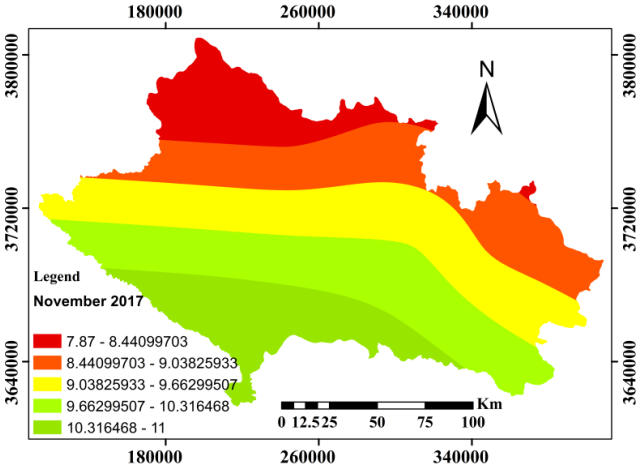
180000
260000
340000
3800000
3720000
3640000
N
Legend
November 2017
7.87 - 8.44099703
8.44099703 - 9.03825933
9.03825933 - 9.66299507
9.66299507 - 10.316468
10.316468 - 11
0 12.525 50 75 100
Km

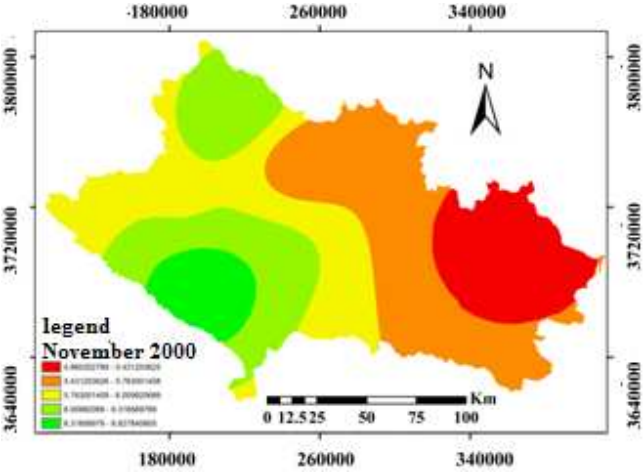
180000
260000
340000
3800000
3720000
3640000
N
legend
November 2000
0 12.525 50 75 100
Km

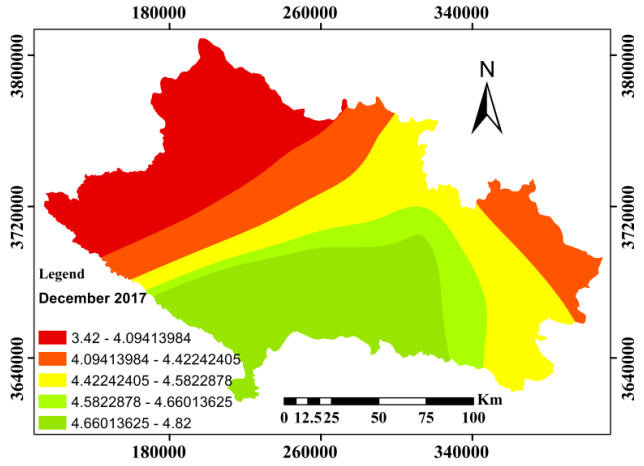
180000
260000
340000
3800000
3720000
3640000
N
Legend
December 2017
3.42 - 4.09413984
4.09413984 - 4.42242405
4.42242405 - 4.5822878
4.5822878 - 4.66013625
4.66013625 - 4.82
0 12.525 50 75 100
Km

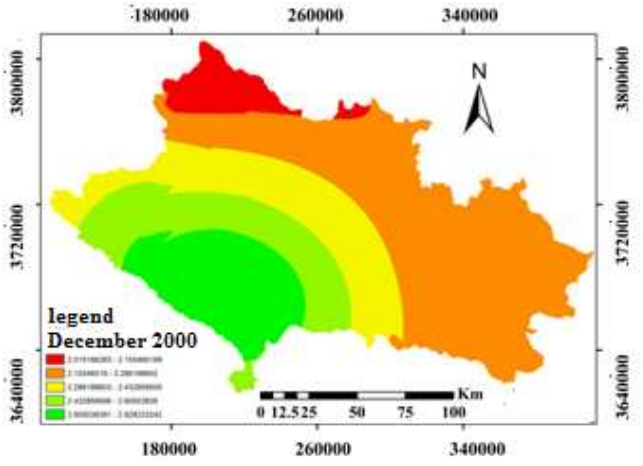
180000
260000
340000
3800000
3720000
3640000
N
legend
December 2000
0 12.525 50 75 100
Km

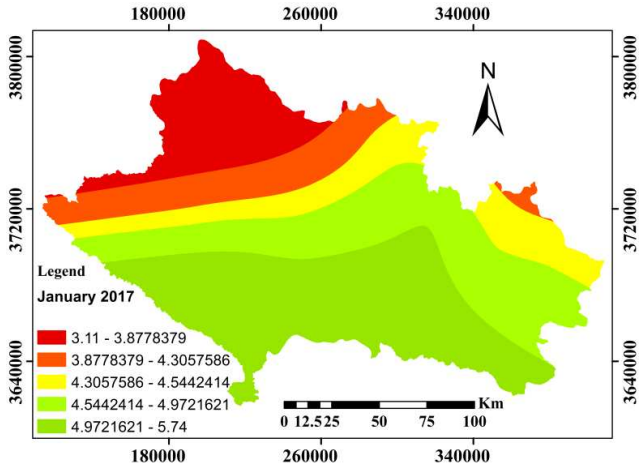
180000
260000
340000
3800000
3720000
3640000
N
Legend
January 2017
3.11 - 3.8778379
3.8778379 - 4.3057586
4.3057586 - 4.5442414
4.5442414 - 4.9721621
4.9721621 - 5.74
0 12.525 50 75 100
Km

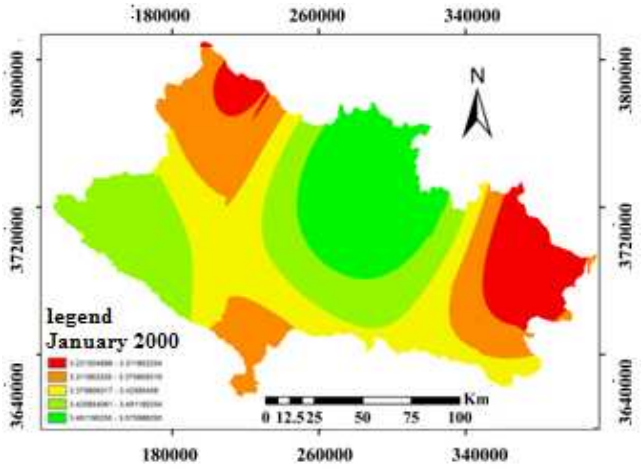
180000
260000
340000
3800000
3720000
3640000
N
legend
January 2000
0 12.525 50 75 100
Km

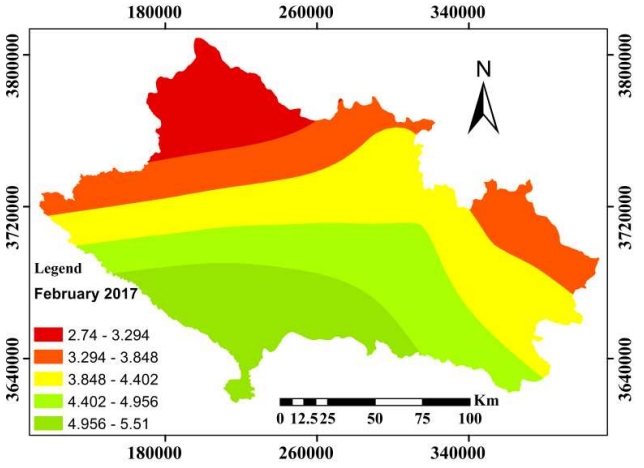
180000
260000
340000
3800000
3720000
3640000
N
Legend
February 2017
2.74 - 3.294
3.294 - 3.848
3.848 - 4.402
4.402 - 4.956
4.956 - 5.51
0 12.525 50 75 100
Km

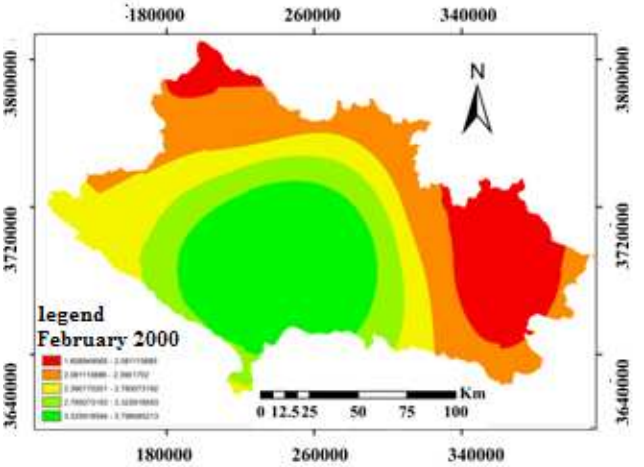
180000
260000
340000
3800000
3720000
3640000
N
legend
February 2000
0 12.525 50 75 100
Km

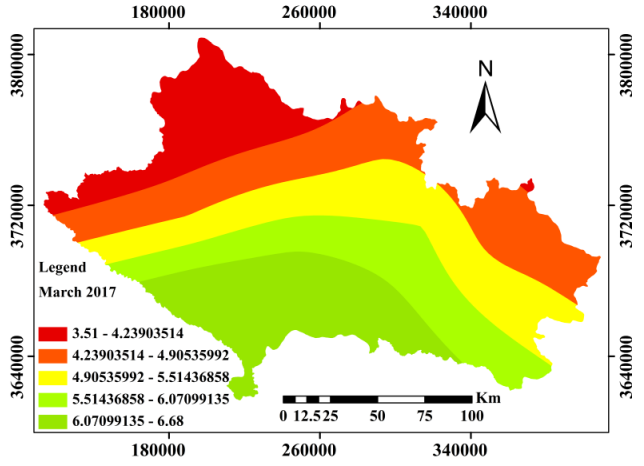
180000
260000
340000
3800000
3720000
3640000
N
Legend
March 2017
3.51 - 4.23903514
4.23903514 - 4.90535992
4.90535992 - 5.51436858
5.51436858 - 6.07099135
6.07099135 - 6.68
0 12.525 50 75 100
Km

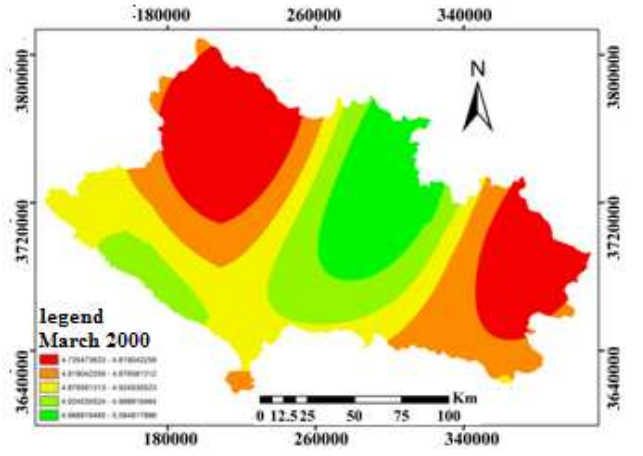
180000
260000
340000
3800000
3720000
3640000
N
legend
March 2000
0 12.525 50 75 100
Km

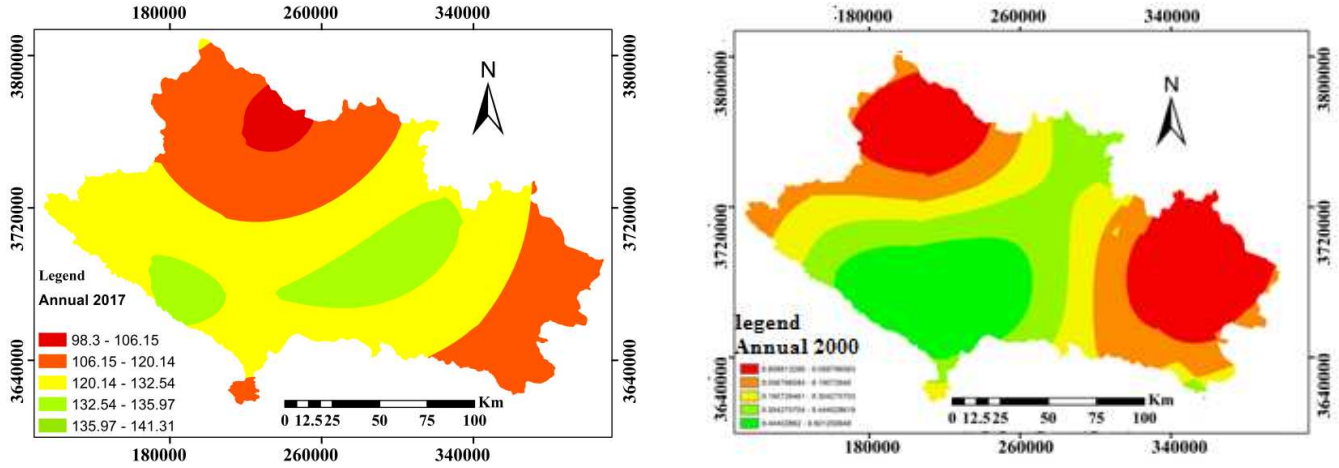

Figure 3: ET0 zoning maps in different time periods in both 2000 and 2017 in Lorestan province

Investigation of the effect of different parameters on ET0

To evaluate the effect of input parameters of ET0 estimation including maximum temperature, minimum temperature, maximum relative humidity, minimum relative humidity, sunshine hours, and wind speed in estimating reference evapotranspiration, multivariate regression analysis between these parameters was done. The results of regression analysis in all study stations showed a pattern of joint influence between inputs and evapotranspiration, the results of Khorramabad for example are shown in Table 4. In this table, the value of multiple correlation coefficient (R), coefficient of determination (R^2), and adjusted coefficient of determination (R^2 Adjusted), analysis of variance, and regression coefficients are shown. In this study, the value of R^2 is equal to 0.952, which indicates the efficiency and accuracy of the model in predicting reference evapotranspiration. One of the important parts of Table (4) is the Beta values and significance level. Observing the level of significance obtained, it can be said that all parameters are significant at the level of one percent and indicates that all input parameters affect the evapotranspiration variable and are used in estimating it. A comparison of the standardized coefficient obtained for the input parameters shows that the maximum temperature with a coefficient of 0.604 has the greatest effect on the reference evapotranspiration and is a stronger predictor than the other variables. After that, wind speed, sunshine hours, minimum temperature, and maximum and minimum relative humidity have the greatest effect on predicting and estimating evapotranspiration, respectively. In studies by de Oliveira et al. (2021) on Amazon basin solar radiation, Lu et al. (2020) on Temperature and precipitation in the Chinese Genhe River Basin, Fu et al. (2022) on China wind speed, and Liu et al. (2022) in the southwest of China temperature and wind speed variables had the greatest effect on ETo which is consistent with the results of the present study. The value of t (both positive and negative) if it is greater than 1.96 and the value of the significance level if it is less than 0.01 shows that the predictor variable has a significant effect on the response variable. According to the values of all six variables, all variables have a significant effect. Nsiah et al. (2021) showed that Linear regression analysis had a good fit with an R^2 of 0.93, indicating that 93% of the variation in observed field-measured ET perfectly matched the ET distributions produced by the SEBAL model.

Table 4. Value of model accuracy coefficients and multivariate regression parameters

Multiple correlation coefficient	Determination coefficient	Corrected determination coefficient	Simulation standard error
0.976	0.952	0.952	0.977

	sum of squares	Degree of freedom	average of squares	F	Significance level
regresion	171076.22	6	28512.703	29842.592	0
residuals	8636.191	9039	0.955		
total	179712.411	9045			

	Not standardized coefficients		Standardized coefficients	t	Significance level
	B	Standard error	Beta		
(Constant)	-0.382	0.114		-3.357	0.001
Tmax	0.25	0.004	0.604	65.827	0
Tmin	0.033	0.004	0.055	6.867	0
RHmax	-0.034	0.001	-0.186	-42.032	0
RHmin	-0. 009	0.001	-0.038	-7.434	0
WS	0.399	0.005	0.212	84.796	0
SUN	0.133	0.005	0.108	26.189	0

Table 3: RMSE of different zoning methods for ET0 in different periods of 2000 and 2017

Zoning methods	2000													2017											
	1	2	3	4	5	6	7	8	9	10	11	12	annual	1	2	3	4	5	6	7	8	9	10	11	12	annual
Ordinary Kriging (Stable)	55.0	87.1	16.2	15.2	31.2	37.1	81.0	9.0	44.0	55.0	4.0	62.0	04.1	84.0	12.1	89.1	24.2	54.2	25.2	14.1	18.1	4.0	69.0	62.0	01.1	15.1
Ordinary Kriging (Circular)	56.0	87.1	16.2	14.2	31.2	37.1	83.0	93.0	44.0	54.0	44.0	62.0	03.1	87.0	22.1	89.1	24.2	54.2	25.2	14.1	18.1	4.0	68.0	62.0	01.1	15.1
Ordinary Kriging (Spherical)	58.0	87.1	16.2	15.2	31.2	37.1	83.0	94.0	44.0	54.0	43.0	62.0	03.1	84.0	16.1	89.1	24.2	54.2	25.2	14.1	18.1	39.0	66.0	6.0	99.0	15.1
Ordinary Kriging (Tetraspherical	58.0	87.1	16.2	15.2	31.2	37.1	82.0	94.0	44.0	54.0	43.0	62.0	03.1	82.0	1.1	89.1	24.2	54.2	25.2	14.1	18.1	38.0	67.0	6.0	98.0	15.1
Ordinary Kriging (Pentaspherical)	59.0	87.1	16.2	16.2	31.2	37.1	81.0	94.0	44.0	54.0	43.0	62.0	03.1	81.0	07.1	89.1	24.2	54.2	25.2	14.1	22.1	38.0	69.0	63.0	98.0	15.1
Ordinary Kriging (Exponential)	67.0	87.1	16.2	16.2	31.2	37.1	82.0	93.0	45.0	54.0	46.0	62.0	02.1	84.0	12.1	89.1	24.2	54.2	25.2	14.1	18.1	4.0	69.0	65.0	1	15.1
Ordinary Kriging (Gaussian)	54.0	87.1	16.2	15.2	31.2	37.1	84.0	9.0	44.0	55.0	4.0	62.0	04.1	86.0	19.1	89.1	24.2	54.2	25.2	14.1	18.1	39.0	67.0	6.0	1	15.1
Ordinary Kriging (Rational Quadratic)	64.0	87.1	16.2	16.2	27.2	36.1	79.0	94.0	45.0	54.0	42.0	62.0	02.1	83.0	08.1	89.1	24.2	54.2	25.2	14.1	21.1	4.0	71.0	63.0	01.1	15.1
Ordinary Kriging (Hole Effect)	39.0	93.1	16.2	17.2	22.2	36.1	76.0	89.0	44.0	55.0	41.0	65.0	04.1	83.0	9.0	45.1	24.2	54.2	25.2	01.1	17.1	38.0	04.1	86.0	98.0	12.1
Ordinary Kriging (K-Bessel)	55.0	87.1	16.2	15.2	31.2	38.1	82.0	9.0	44.0	55.0	4.0	62.0	04.1	84.0	11.1	89.1	24.2	54.2	25.2	14.1	18.1	39.0	69.0	62.0	01.1	15.1
Ordinary Kriging (J-Bessel)	46.0	91.1	16.2	17.2	21.2	36.1	76.0	89.0	44.0	55.0	42.0	64.0	04.1	9.0	9.0	38.1	24.2	54.2	25.2	97.0	16.1	36.0	06.1	81.0	99.0	07.1
Simple Kriging (Stable)	8.0	7.1	94.1	03.2	08.2	31.1	75.0	84.0	44.0	49.0	58.0	55.0	96.0	8.0	15.1	66.1	98.1	28.2	97.1	02.1	08.1	39.0	71.0	73.0	95.0	04.1
Simple Kriging (Circular)	8.0	7.1	94.1	03.2	08.2	31.1	75.0	84.0	44.0	49.0	57.0	55.0	96.0	8.0	15.1	66.1	98.1	28.2	97.1	02.1	08.1	39.0	71.0	73.0	95.0	04.1
Simple Kriging (Spherical)	79.0	7.1	94.1	03.2	08.2	31.1	75.0	84.0	43.0	49.0	53.0	55.0	96.0	8.0	15.1	66.1	98.1	28.2	97.1	02.1	08.1	39.0	71.0	73.0	95.0	04.1
Simple Kriging (Tetraspherical)	77.0	7.1	94.1	03.2	07.2	3.1	75.0	84.0	43.0	49.0	5.0	55.0	96.0	8.0	15.1	66.1	98.1	28.2	97.1	02.1	08.1	39.0	71.0	73.0	95.0	04.1
Simple Kriging (Pentaspherical)	75.0	7.1	94.1	03.2	07.2	29.1	75.0	85.0	42.0	49.0	48.0	55.0	96.0	8.0	15.1	66.1	98.1	28.2	97.1	02.1	08.1	39.0	71.0	73.0	95.0	04.1
Simple Kriging (Exponential)	8.0	7.1	94.1	03.2	08.2	31.1	75.0	84.0	44.0	49.0	59.0	55.0	96.0	8.0	15.1	66.1	98.1	28.2	97.1	02.1	08.1	39.0	71.0	73.0	95.0	04.1
Simple Kriging (Gaussian)	8.0	7.1	94.1	03.2	08.2	31.1	75.0	84.0	44.0	49.0	58.0	55.0	96.0	8.0	15.1	66.1	98.1	28.2	97.1	02.1	08.1	39.0	71.0	73.0	95.0	04.1
Simple Kriging (Rational Quadratic)	79.0	7.1	94.1	03.2	08.2	3.1	75.0	83.0	44.0	49.0	57.0	55.0	96.0	8.0	15.1	66.1	98.1	27.2	97.1	02.1	08.1	39.0	71.0	73.0	95.0	04.1
Simple Kriging (Hole Effect)	36.0	7.1	94.1	02.2	05.2	18.1	75.0	87.0	4.0	49.0	34.0	55.0	94.0	67.0	95.0	3.1	97.1	32.2	97.1	96.0	08.1	34.0	59.0	54.0	9.0	99.0
Simple Kriging (K-Bessel)	8.0	7.1	94.1	03.2	08.2	31.1	75.0	84.0	44.0	49.0	57.0	55.0	96.0	8.0	15.1	66.1	98.1	28.2	97.1	02.1	08.1	39.0	71.0	73.0	95.0	04.1
Simple Kriging (J-Bessel)	37.0	67.1	93.1	01.2	04.2	2.1	74.0	92.0	38.0	48.0	38.0	54.0	93.0	63.0	87.0	34.1	96.1	34.2	96.1	91.0	07.1	29.0	55.0	51.0	83.0	97.0
Universal Kriging (Stable)	55.0	87.1	16.2	15.2	31.2	37.1	81.0	9.0	44.0	55.0	4.0	62.0	04.1	84.0	12.1	89.1	24.2	54.2	25.2	14.1	18.1	4.0	69.0	62.0	01.1	15.1
Universal Kriging (Circular)	56.0	87.1	16.2	14.2	31.2	37.1	83.0	93.0	44.0	54.0	44.0	62.0	03.1	87.0	22.1	89.1	24.2	54.2	25.2	14.1	18.1	4.0	68.0	62.0	01.1	15.1
Universal Kriging (Spherical)	57.0	87.1	16.2	15.2	31.2	37.1	83.0	94.0	44.0	54.0	43.0	62.0	03.1	84.0	16.1	89.1	24.2	54.2	25.2	14.1	18.1	39.0	66.0	6.0	99.0	15.1
Universal Kriging (Tetraspherical)	58.0	87.1	16.2	15.2	31.2	37.1	82.0	94.0	44.0	54.0	43.0	62.0	03.1	82.0	1.1	89.1	24.2	54.2	25.2	14.1	18.1	38.0	67.0	6.0	98.0	15.1
Universal Kriging (Pentaspherical)	6.0	87.1	16.2	16.2	31.2	37.1	81.0	94.0	44.0	54.0	43.0	62.0	03.1	81.0	07.1	89.1	24.2	54.2	25.2	14.1	22.1	38.0	69.0	63.0	98.0	15.1
Universal Kriging (Exponential)	67.0	87.1	16.2	16.2	31.2	37.1	82.0	93.0	45.0	54.0	46.0	62.0	02.1	84.0	12.1	89.1	24.2	54.2	25.2	14.1	18.1	4.0	69.0	65.0	1	15.1
Universal Kriging (Gaussian)	54.0	87.1	16.2	15.2	31.2	37.1	84.0	9.0	44.0	55.0	4.0	62.0	04.1	86.0	19.1	89.1	24.2	54.2	25.2	14.1	18.1	39.0	67.0	6.0	1	15.1
Universal Kriging (Rational Quadratic)	64.0	87.1	16.2	16.2	27.2	36.1	79.0	94.0	45.0	54.0	42.0	62.0	02.1	83.0	08.1	89.1	24.2	54.2	25.2	14.1	21.1	4.0	71.0	63.0	01.1	15.1
Universal Kriging (Hole Effect)	39.0	93.1	16.2	17.2	22.2	36.1	76.0	89.0	44.0	55.0	41.0	65.0	04.1	83.0	9.0	45.1	24.2	54.2	25.2	01.1	17.1	38.0	04.1	86.0	98.0	12.1
Universal Kriging (K-Bessel)	55.0	87.1	16.2	15.2	31.2	38.1	82.0	9.0	44.0	55.0	4.0	62.0	04.1	84.0	11.1	89.1	24.2	54.2	25.2	14.1	18.1	39.0	69.0	62.0	01.1	15.1
Universal Kriging (J-Bessel)	46.0	91.1	16.2	17.2	21.2	36.1	76.0	89.0	44.0	55.0	42.0	64.0	04.1	9.0	9.0	38.1	24.2	54.2	25.2	97.0	16.1	36.0	06.1	81.0	99.0	07.1
IDW power 1	83.0	94.1	27.2	14.2	2.2	37.1	83.0	9.0	47.0	54.0	65.0	63.0	02.1	88.0	25.1	75.1	39.2	74.3	38.2	09.1	2.1	42.0	76.0	78.0	05.1	14.1
IDW power 2	76.0	01.2	37.2	16.2	2.2	34.1	82.0	88.0	46.0	58.0	56.0	64.0	03.1	85.0	19.1	62.1	57.2	02.3	64.2	05.1	18.1	42.0	72.0	72.0	03.1	12.1
IDW power 3	73.3	1.2	5.2	32.2	29.2	4.1	83.0	94.0	47.0	63.0	54.0	66.0	08.1	85.0	16.1	59.1	75.2	28.3	87.2	02.1	17.1	42.0	7.0	69.0	04.1	12.1
GPI	62.0	94.1	62.2	27.2	3.2	74.1	01.1	96.0	4.0	65.0	54.0	77.0	14.1	87.0	28.1	48.1	82.2	9.2	36.2	01.1	11.1	44.0	68.0	63.0	95.0	02.1
LPI	48.0	97.1	6.2	4.2	37.2	65.1	9.0	02.1	42.0	69.0	54.0	7.0	11.1	62.0	07.1	56.1	08.3	32.3	74.2	99.0	06.1	28.0	54.0	45.0	76.0	04.1
RBF	38.0	92.1	3.2	18.2	23.2	37.1	76.0	9.0	45.0	56.0	37.0	63.0	02.1	73.0	84.0	42.1	53.2	87.2	49.2	97.0	15.1	33.0	67.0	56.0	91.0	04.1

4. Conclusion

This study was conducted to investigate the trend of temporal and spatial changes in reference evapotranspiration and investigate the effect of meteorological parameters on it in 18 years (2000-2017) in Lorestan province in western Iran. The reason for choosing this period was the completeness of the information of all synoptic stations in the studied stations to estimate the reference evapotranspiration. The Mankendall test was used to examine the trend of temporal changes and to investigate the spatial distribution, interpolation methods were used with the help of GIS. The results of the Mankendall test showed that in most months of the year in different stations the trend of ET0 changes has been decreasing. The annual trend has also decreased in stations except for Aleshtar, Noorabad, and Poldokhtar stations. It was also found that February has the lowest trend and April has the highest trend and among the stations in the province, Aleshtar station has the highest, and Azna station has the lowest trend in ET0 changes. In general, it can be said that the trend of ET0 changes in Lorestan province has decreased in the study period. to zone ET0 in Lorestan province, different zoning methods were evaluated using the cross-validation method. The results showed that the Simple Kriging (J-Bessel) method for ET0 zoning in May, June, July, August, October, December, January, March, and annually in 2000 and June, July, September, October, and annually in 2017, the LPI method for zoning in April, November, December, January, February and March in 2017, Simple Kriging method (Hole Effect) for zoning In April, September and February of 2000, the Simple Kriging (Rational Quadratic) method for zoning in November 2000 and August 2017 and the RBF method for zoning in May 2017, as appropriate The most models were selected. After selecting the appropriate method, zoning was performed. Zoning showed that the maximum amount of ET0 occurs in the south of the province and has decreased by moving to the north and east of the province. These results indicate that the geographical location determines the spatial distribution of ET0 through changes in latitude and topographic conditions. Finally, the effect of different meteorological parameters in estimating reference evapotranspiration was investigated. The results of this study showed a common pattern of the effect of six parameters on evapotranspiration in all 9 stations studied. Accordingly, the maximum temperature had the greatest effect on the reference evapotranspiration and the temporal-spatial variation of ET0 was most affected by this parameter. Investigation of temporal changes and spatial distribution of reference evapotranspiration can be important in better management and planning of water resources, the necessary information for hydrological studies at the regional level, design of irrigation systems, and determination of irrigation hydro modules. Given the importance of these issues, especially in the agricultural sector, and the strategic position of Lorestan province in the country as one of the agricultural hubs, the need for comprehensive studies in the field of evapotranspiration is suggested.

Conflict of interest

Authors do not feel there is any conflict, disclosure of relationships and interests provides a more complete and transparent process, leading to an accurate and objective assessment of the work. Awareness of a real or perceived conflict of interest is a perspective to which the readers are entitled. This is not meant to imply a financial relationship with an organization. The authors declare that they have no conflict of interest.

Funding

The authors declare no funding source.

References

Allen, G. R., Pereira, S. L., Raes, D. and Smith, M. (1998). Crop evapotranspiration, Guidelines for computing crop water requirement, FAO Irrigation and Drainage Paper 56, Rome, Italy.

Antal, A., Guerreiro, P. M. and Cheval, S. (2021). Comparison of spatial interpolation methods for estimating the precipitation distribution in Portugal. Theoretical and Applied Climatology, 145(3), 1193-1206.

Chang, Y., Ding, Y., Zhang, S., Qin, J., & Zhao, Q. (2023). Variations and drivers of evapotranspiration in the Tibetan Plateau during 1982–2015. Journal of Hydrology: Regional Studies, 47, 101366.

de Oliveira, R. G., Júnior, L. C. G. V., da Silva, J. B., Espíndola, D. A., Lopes, R. D., Nogueira, J. S. and Rodrigues, T. R. (2021). Temporal trend changes in reference evapotranspiration contrasting different land uses in southern Amazon basin. Agricultural Water Management, 250, 106815, 1-14.

Djaman, K. B., Balde, A., Sow, A., Muller, B., Irmak, S. K., N'Diaye, M., Manneh, B. D., Moukoumbi, Y., Futakuchi, K. and Saito, K. (2015). Evaluation of sixteen reference Evapotranspiration methods under sahelian conditions in the Senegal River Valley, Hydrological Regional Stududies, 3: 139-159.

Fu, J., Gong, Y., Zheng, W., Zou, J., Zhang, M., Zhang, Z., ... & Quan, B. (2022). Spatial-temporal variations of terrestrial evapotranspiration across China from 2000 to 2019. Science of The Total Environment, 825, 153951.

Gaus, I., Kinniburgh, D., Talbot, J. and Webster, R. (2003). Geostatistical analysis of arsenic concentration in groundwater in Bangladesh using disjunctive Kriging, Environmental Geology, 44: 939-948.

Gibrilla, A., Anornu, G. and Adomako, D. (2018). Trend analysis and ARIMA modelling of recent groundwater levels in the White Volta River basin of Ghana. Groundwater for Sustainable Development, 6, 150-163.

Grismer, M. E., Orang, M., Snyder, R. and Matyac, R. (2002). Pan evaporation to reference evapotranspiration conversion methods. Journal of Irrigation and drainage Engineer, 128(3), 180-184.

Hargreaves, G. H. (1994). Defining and using reference evapotranspiration, Journal of Irrigation and Drainage Engineering. 12(6): 1132-1139.

Kendall, M. G. (1975). Rank Correlation Methods, Charles Griffin, London (1975).

Liu, Y., Lian, J., Luo, Z., & Chen, H. (2022). Spatiotemporal variations in evapotranspiration and transpiration fraction following changes in climate and vegetation in a karst basin of southwest China. Journal of Hydrology, 612, 128216.

Lu, X., Zang, C., & Burenina, T. (2020). Study on the variation in evapotranspiration in different period of the Genhe River Basin in China. Physics and Chemistry of the Earth, Parts A/B/C, 120, 102902., 1-36

Mann, H. B. (1945). Nonparametric tests against trend, Econometrical, Journal of the Econometric Society, 245-259.

Mehdizadeh, S., Behmanesh, J. and Khalili, K. (2017). Using MARS, SVM, GEP and empirical equations for estimation of monthly mean reference evapotranspiration, Computers and Electronics in Agriculture, 139, 103-114.

Nam, W. H., Hong, E. M. and Choi, J. Y. (2015). Has climate change already affected the spatial distribution and temporal trends

of reference evapotranspiration in South Korea, Agricultural Water Management, 150: 129-138.

Nsiah, J. J., Gyamfi, C., Anornu, G. K. and Odai, S. N. (2021). Estimating the spatial distribution of evapotranspiration within the Pra River Basin of Ghana. Heliyon, 7(4), e06828, 1-10.

Paredes, P., Pereira, L. S., Almorox, J. and Darouich, H. (2020). Reference grass evapotranspiration with reduced data sets: Parameterization of the FAO Penman-Monteith temperature approach and the Hargeaves-Samani equation using local climatic variables. Agricultural Water Management, 240, 106210, 1-23.

Prăvălie, R., Piticar, A., Roșca, B., Sfîcă, L., Bandoc, G., Tiscovschi, A. and Patriche, C. (2019). Spatio-temporal changes of the climatic water balance in Romania as a response to precipitation and reference evapotranspiration trends during 1961–2013, Catena, 172, 295-312.

Samuel, A., Girma, A., Zenebe, A. and Ghebreyohannes, T. (2018). Spatio-temporal variability of evapotranspiration and crop water requirement from space, Journal of hydrology, 567, 732-742.

Shao, Y., Liu, H., Du, Q., Liu, Y., & Sun, J. (2022). Seasonal variation and controlling factors of evapotranspiration over a "floating blanket" wetland in southwest China. Journal of Hydrology, 612, 128316.

Tabari, H., Marofi, S., Aeini, A., HosseinzadehTalaeea, P. and Mohammadi, K. (2011). Trend analysis of reference evapotranspiration in the western half of Iran, Agriculture Forest Meteorology, 151 (2): 128-136.

Tang, Y., & Tang, Q. (2021). Variations and influencing factors of potential evapotranspiration in large Siberian River basins during 1975–2014. Journal of Hydrology, 598, 126443.

Wang, L., Wang, G., Xue, B., Yinglan, A., Fang, Q., & Shrestha, S. (2022). Spatiotemporal variations in evapotranspiration and its influencing factors in the semiarid Hailar river basin, Northern China. Environmental Research, 212, 113275.

Wang, Q. F., Tang, J., Zeng, J. Y., Qu, Y. P., Zhang, Q., Shui, W., Wang, W. L., Yi, L. and Leng, S. (2018). Spatial-temporal evolution of vegetation evapotranspiration in Hebei Province, China, Journal of integrative agriculture, 17(9), 2107-2117.

Yang, W., Zhao, Y., Wang, D., Wu, H., Lin, A. and He, L. (2020). Using principal components analysis and IDW interpolation to determine spatial and temporal changes of surface water quality of Xin'anjiang river in Huangshan, China. International journal of environmental research and public health, 17(8), 2942, 1-14.

Zhao, T., Zhu, Y., Ye, M., Yang, J., Jia, B., Mao, W. and Wu, J. (2022). A new approach for estimating spatial-temporal phreatic evapotranspiration at a regional scale using NDVI and water table depth measurements. Agricultural Water Management, 264, 107500.

Zongxing, L., Qi, F., Wei, L., Tingting, W., Yan, G., Yamin, W., Aifang, C., Jingguo, L. and Li, L. (2015). Spatial and temporal trend of potential evapotranspiration and related driving forces in Southwestern China, during 1961-2009, Quaternary International 336: 127-144.